Partition-based Network Equivalent Method for Power System Subsynchronous Oscillation Analysis

Chenxuan Wang, Weimin Zheng, Zhen Wang, Yangqing Dan, and Ping Ju

***Abstract*—Given large-scale modern power systems with power electronic converters, the numerical simulation with subsynchronous oscillation (SSO) faces great challenges in engineering practice due to sharply enlarged modeling scale and high computational burden. To reduce the modeling scale, network partition and equivalent becomes a vital technique in numerical simulations. Although several methods have been developed for network equivalent, a generally accepted rule for network partition is still required. This paper proposes that the system can be partitioned into three parts, i.e., the internal, the middle, and the external subsystems, in which the internal subsystem consists of all power electronic components, the middle subsystem includes those selected AC dynamic components with detailed models, and the remaining components and buses constitute the external subsystem. The external subsystem is further represented by an equivalent RLC network determined by the frequency dependent network equivalent (FDNE) method. In the proposed method, the observability index and the electrical distance index are used to identify the interface between the middle and the external subsystems. Case studies based on a modified Hydro-Quebec system are used to verify the effectiveness of the proposed method.**

***Index Terms*—Electrical distance, network equivalent, subsynchronous oscillation, observability index.**

I. Introduction

NOWADAYS, the proliferation of power electronic converters in modern power systems brings about several new types of subsynchronous oscillation (SSO) problems associated with the interaction between converter controller and the AC power grid, which has aroused great concern among industry and academia. The studies of SSO require the detailed electromagnetic transient (EMT) models of related components in the system, and then the EMT simulation program [1], [2] is adopted to compute and analyze the SSO trajectory. However, if each component of the whole system is modeled in full details, the computation and modeling for SSO studies will be quite burdensome [3]. Hence, it is a common practice to partition the whole power grid into several subsystems. Parts of these subsystems are represented by detailed models and the EMT dynamics for SSO analysis can be fully captured by these models, i.e., the phase-locked loop, and the DC voltage and the AC current control loops of the power electronic converters should be modeled in detail [4]. Meanwhile, part of these subsystems can be represented by an reduced-order equivalent system, which preserves the transient characteristics of the original system [5]. However, there exist the following two problems to be solved.

1) Network partition and interface identification between subsystems, which means the location of interface buses between different subsystems needs to be identified.

2) Network equivalent representation that has similar electrical characteristics to the original one.

For the first problem, a type of two-part partition method has been widely used in the existing studies, in which the whole power system is partitioned into the internal and the external subsystems. The internal subsystem usually includes the power electronic converters associated with the studied SSO phenomenon with their detailed EMT dynamics modelled [1], whereas the external subsystem is usually composed of a conventional AC grid represented by an ideal voltage source in series with a constant equivalent impedance, for the purpose of system order reduction [6], [7]. In this way, the computational burden of SSO analysis can be greatly reduced.

As for the second problem, the following two types of methods have been developed: ① the conventional Thevenin (or Norton) equivalent which is represented by an ideal voltage source in series with some equivalent impedance [8]; and ② the frequency dependent network equivalent (FDNE) [9] which is represented by some RLC equivalent circuits. The former is easy for implementation, but its equivalent scheme is only effective at the fundamental frequency band.

Manuscript received: August 15, 2022; revised: February 10, 2023; accepted: April 17, 2023. Date of CrossCheck: April 17, 2023. Date of online publication: June 1, 2023.

This work was jointly supported by the Science and Technology Project of State Grid Zhejiang Electric Power Co., Ltd. (No. 5211JY21N001) and the National Natural Science Foundation of China (No. 51837004).

C. Wang and Z. Wang (corresponding author) are with the Department of Electrical Engineering, Zhejiang University, Hangzhou 310027, China (e-mail: 11710035@zju.edu.cn; eezwang@ieee.org).

W. Zheng and Y. Dan are with the Economic Research Institute of State Grid Zhejiang Electric Power Co., Ltd., Hangzhou 310016, China (e-mail: zwmhappy@126.com; danyangqing@aliyun.com).

P. Ju is with the College of Energy and Electrical Engineering, Hohai Universtiy, Nanjing 211100, China, and he is also with the Department of Electrical Engineering, Zhejiang University, Hangzhou 310027, China (e-mail: pju@hhu.edu.cn).

DOI: 10.35833/MPCE.2022.000517

In contrast, the equivalent scheme of the latter can maintain the original system characteristics in a wide frequency band. The zero-pole matching method [7] and the vector-fitting (VF) based rational approximation [10] can be attributed to this category.

However, there are some problems in the above two-part partition method. On the one hand, though the system scale is reduced by replacing a large portion of the power system by a linear equivalent system, the nonlinear dynamics outside the internal subsystem cannot be presented completely [11]. Thus, the simulation accuracy will be affected. On the other hand, the network partitioning is mainly based on engineering judgment, and a generally accepted rule for it is still required [12].

In this paper, a three-part partition method is developed including the internal, the middle, and the external subsystems, and the interfaces among these subsystems are quantitatively identified. The conventional FDNE method is then applied to determine the equivalent RLC network representing the external subsystem. The contributions of this paper can be summarized as follows.

1) A three-part partition method is proposed for SSO analysis, in which the whole system can be partitioned into three subsystems to reduce the computational burden.

2) An observability index is introduced to identify the best observation bus related to each dominant SSO mode and an electrical distance (ED) index is used to quantify the electrical proximity degrees between any bus in the system and the "best observation buses".

3) A frequency-domain equivalent model based on the FDNE method is introduced for network equivalent, in which the frequency response characteristic of the target network within the whole subsynchronous frequency band can be retained.

The remainder of this paper is organized as follows. In Section II, the network partition and interface identification are presented. Section III presents case studies and validates the method through a test system, and Section IV summarizes the paper.

II. Network Partition and Interface Identification

A. Network Partition Framework

The network partition framework is illustrated in Fig. 1.

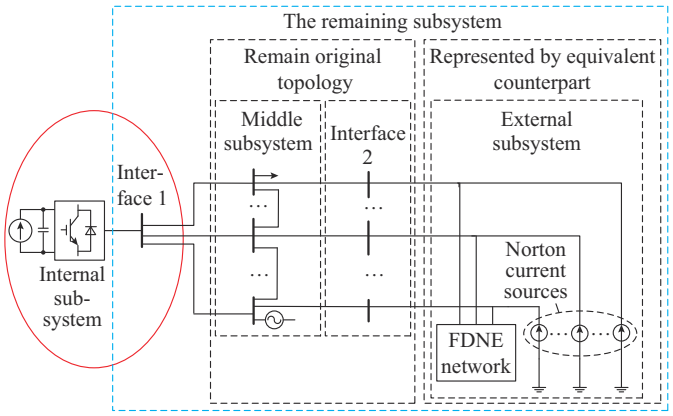

Fig. 1. Network partition framework.

1) The internal subsystem: this subsystem mainly consists of those power electronic converters modelled in details, including the corresponding points of common coupling (PCCs), in particular, those having high participation factors related to some SSO dynamics should be modeled with adequate degree of details [3].

2) The middle subsystem: this subsystem is topologically directly connected to the internal subsystem, which mainly preserves the EMT dynamics of those conventional power system components such as synchronous generator and asynchronous motor. For example, the stator and the rotor transient dynamics of synchronous motors and the detailed exciter dynamics should be modelled, while the dynamics of the prime mover is ignored or a constant mechanical power can be simply used due to its much slower dynamic behavior [13].

3) The external subsystem: the remaining components and buses constitute the external subsystem. Since this subsystem is not directly connected to the internal subsystem, the studied SSO phenomenon within the former has minor effect on the latter's transient behavior, and vice versa [14]. To reduce the system scale, this subsystem is considered to be replaced by an equivalent system, and an FDNE system is adopted in this paper, which is introduced in Appendix A.

Since the FDNE system can only present the characteristics of a linear and time-invariant system, the simplification of the following dynamic components in this subsystem should be accomplished.

1) Each passive dynamic component, e. g., asynchronous motor, is represented by a constant impedance model.

2) Each active dynamic component is represented by a fundamental frequency voltage source behind a reactance.

The above treatments make the external subsystem a linear and time-invariant system [14]. To reduce its order, the external subsystem is further represented by an equivalent counterpart consisting of several Norton current sources and an FDNE system, as illustrated in Fig. 1 [5]. The Norton current source, which connects to each port of the FDNE system, can be easily determined by Norton's theorem procedure on the original external subsystem [8]. The admittance network is a passive RLC circuit, whose parameters are determined by those VF methods [10], [15].

1) Interface 1: interface 1 is a kind of the internal subsystem bus which has a direct connection to the middle subsystem. In this paper, the group of all the grid-connected buses of these converters is regarded as interface 1.

2) Interface 2: interface 2 is a set of middle subsystem buses that have a direct connection to the external subsystem, which will be identified based on the following observability index [16] and the ED index.

B. Interface Identification

Since interface 1 can be directly determined by the electrical topology according to Section II-A, in the following, an observability index and the ED index are introduced to determine interface 2.

1) The Best Observation Bus

According to the modal decomposition theory, any output

trajectory of transient system after disturbance can be determined by SSO modes when the system nonlinearity is ignored [17]. In other words, if the dominant SSO modes can be kept before and after equivalence, the original SSO trajectory profiles can be maintained. To this regard, the concept of mode observability is introduced here so that the dominant SSO modes can be traced after equivalence.

Supposing that the time-domain trajectory of the i^{th} nodal voltage $v_i(t)$ excited by the disturbance can be expressed as:

$$v_i(t) \approx \sum_{m=1}^{M} V_i^m \exp(\lambda_m t) \tag{1}$$

where $i = 1, 2, \ldots, N$ and N is the total number of buses; λ_m is the m^{th} dominant SSO mode; M is the total number of dominant SSO modes; and V_i^m is the corresponding voltage magnitude. The SSO mode observability index θ_i^m is firstly defined in [16], which is used to identify interface 1:

$$\theta_i^m = \frac{V_i^m}{\sum_{k=1}^{N} V_k^m} \tag{2}$$

where k represents the corresponding best observation bus index in S_O, and S_O represents the bus index set of all best observation buses corresponding to the dominant SSO modes.

The observability index can quantify the participation degree of the m^{th} dominant SSO mode observed by the i^{th} nodal voltage signal. However, computing θ_i^m via (2) by a full-detailed EMT simulation is not practical, instead, a non-simulation index is introduced below.

Considering the nodal admittance matrix $\boldsymbol{Y}(s)$, the following similarity transformation can be applied:

$$\boldsymbol{Y}(s) = \boldsymbol{L}\boldsymbol{\Lambda}\boldsymbol{R} \tag{3}$$

where $\boldsymbol{\Lambda}$ is the diagonal eigenvalue matrix; and $\boldsymbol{L}$ and $\boldsymbol{R}$ are the left and right eigenvector matrices, respectively. According to the definition, $\boldsymbol{Y}(\lambda_m)$ at frequency $s = \lambda_m$ is a singular matrix, i.e., a zero eigenvalue exists in $\boldsymbol{\Lambda}$, which is actually a very small value close to zero due to computational error. Let r_m represent the row index corresponding to the diagonal element with the smallest modular value in $\boldsymbol{\Lambda}$. According to [16], an equivalent θ_i^m with (2) can be obtained as:

$$\theta_i^m = \left| L_{i,r_m} \right| \Big/ \sum_{k=1}^{N} \left| L_{k,r_m} \right| \tag{4}$$

where L_{i,r_m} represents the element of the i^{th} row and r_m^{th} column of the matrix $\boldsymbol{L}$; and L_{k,r_m} represents the element of the k^{th} row and r_m^{th} column of the matrix $\boldsymbol{L}$. The larger the θ_i^m, the more obviously the m^{th} dominant SSO mode can be observed at bus i [16].

The bus with the largest θ_i^m is referred to as the best observation bus associated with the m^{th} dominant SSO mode.

2) ED Index

ED is a widely used index to measure the electrical proximity and quantify the connection tightness between two buses in a power system [18]. The ED value d_{ij} between bus i and bus j is defined as [19]:

$$d_{ij} = \left| (Z_{ii} - Z_{ij}) - (Z_{ji} - Z_{jj}) \right| \tag{5}$$

where Z_{ii}, Z_{ij}, Z_{ji}, and Z_{jj} are the impedance matrix elements between these two buses.

3) Critical ED (CED)

In this paper, a CED index is used to screen out those buses in the whole system with tight connection with the "best observation bus" of each dominant SSO modes. For each $k \in S_O$, let Z_{kk} represent the k^{th} diagonal element of the nodal impedance matrix, whose magnitude is the Thevenin impedance observed from the bus k, which can be regarded as the ED between the bus k and the ground, i.e., the infinite bus. The CED value D_k corresponding to bus k can be defined in (6), as illustrated in Fig. 2, and the middle and the external subsystems can be identified based on (6).

$$D_k = \left| Z_{kk} \right| \quad k \in S_O \tag{6}$$

It can be found that D_k and the short circuit ratio (SCR) value SCR_k at bus k also satisfy the following relationship:

$$SCR_k = \frac{1}{\left| Z_{kk} \right|} = \frac{1}{D_k} \tag{7}$$

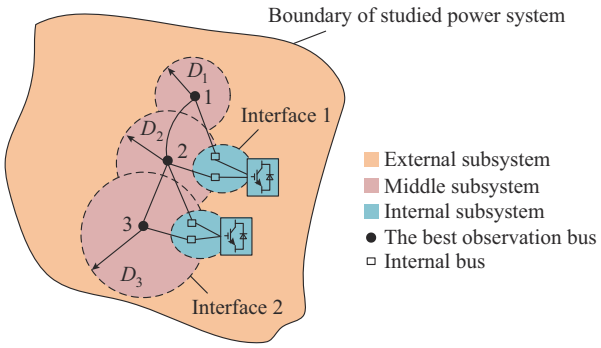

Fig. 2. CED-based network partition.

4) Network Partition Procedure

The complete network partition procedure is explained as follows.

Step 1: internal subsystem identification. All converter-interface-based devices integrated into the grid are classified into the internal subsystem devices, which are in the blue region shown in Fig. 2. All grid-connected or PCC buses for converters are regarded as buses in interface 1.

Step 2: dominant SSO mode evaluation. The dominant SSO modes are evaluated by some mode analysis methods, e.g., the participation factor method.

Step 3: the best observation bus identification. For each dominant SSO mode, calculate the observability index for each bus based on (4) and the bus with the maximum value of observability index is regarded as the best observation bus, as illustrated in Fig. 2, according to which S_O is determined.

Step 4: ED and CED calculation. According to (5), the ED d_{kj} between any bus $k \in S_O$ and any bus $j \in U$ in the remaining system (all buses excluding those in the internal subsystem and interface 1) is calculated, where U represents the bus index set of remaining system. The corresponding D_k is further calculated based on (6).

Step 5: middle and external subsystem identification. Given the internal subsystem determined in *Step 1*, for any dominant SSO mode, let k represents its corresponding best ob-

servation bus index in S_O, all buses in set U in the remaining systems are grouped according to the following rule: $\forall j \in U$, if $d_{kj} \leq D_k$, then j is grouped into the middle subsystem set.

In this paper, all buses above are traversed and S_M is the bus index set of the final middle subsystem. Thus, the bus index set of external subsystem S_E can be determined by set difference operation $S_E = U \backslash S_M$. The relationship between the middle and the external subsystems is illustrated in Fig. 2. It should be noted that the affiliated equipments (generators, converts, loads, etc.) with buses in S_M and S_E are also grouped into the middle and the external subsystems, respectively.

As described in Section II-A, the collection of the middle subsystem buses with the direct connection to the external subsystem is regarded as the desired interface 2.

Step 6: FDNE system. After the network partition, an N-port external subsystem should be replaced by an equivalent RLC network to reduce the system scale. Figure 3(a) shows a typical N-port equivalent circuit, which consists of two parts: ① constant current sources $\boldsymbol{I}=[i_1, i_2, \ldots, i_N]$, and ② passive admittance components, i. e., $y_{ii}(s)$, $y_{ij}(s)$, and $y_{jj}(s)$. Since the contribution of the active components in the external subsystem on the transient dynamics of the internal subsystem is only limited to the fundamental frequency, the current sources are also constructed only considering the fundamental frequency [14]. The passive admittance network is modeled by FDNE considering its characteristics over a specific bandwidth. The structure of FDNE is illustrated in Fig. 3(b). Details of the FDNE method are introduced in the Appendix A.

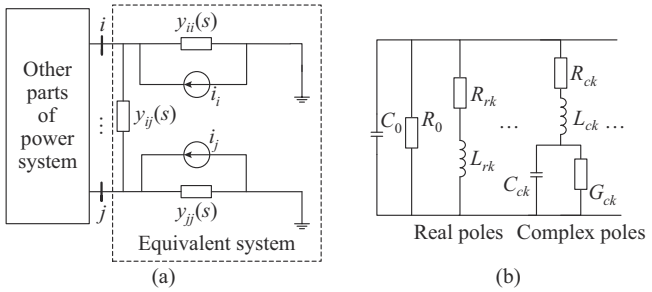

Fig. 3. Equivalent RLC network of external subsystem. (a) Typical N-port equivalent circuit. (b) Structure of FDNE.

III. Case Studies

In Fig. 4, a modified Hydro-Quebec system in [20] is used as a target power system to test the proposed method, by adding an additional 1000 MW type-4 wind farm system, which is simply modeled as a grid-side converter with an LC filter integrated at an additional bus 30 (B30). And B30 is connected to B1 via a step-up transformer. In the system, there are 7 synchronous generators and 2 induction machines. All loads are modeled as constant impedance. The system topology and all operational data can be found in [20]. Details of the wind farm system such as the controller structure and parameters can be referred to in [21]. In Fig. 4, ASG stands for asynchronous generator.

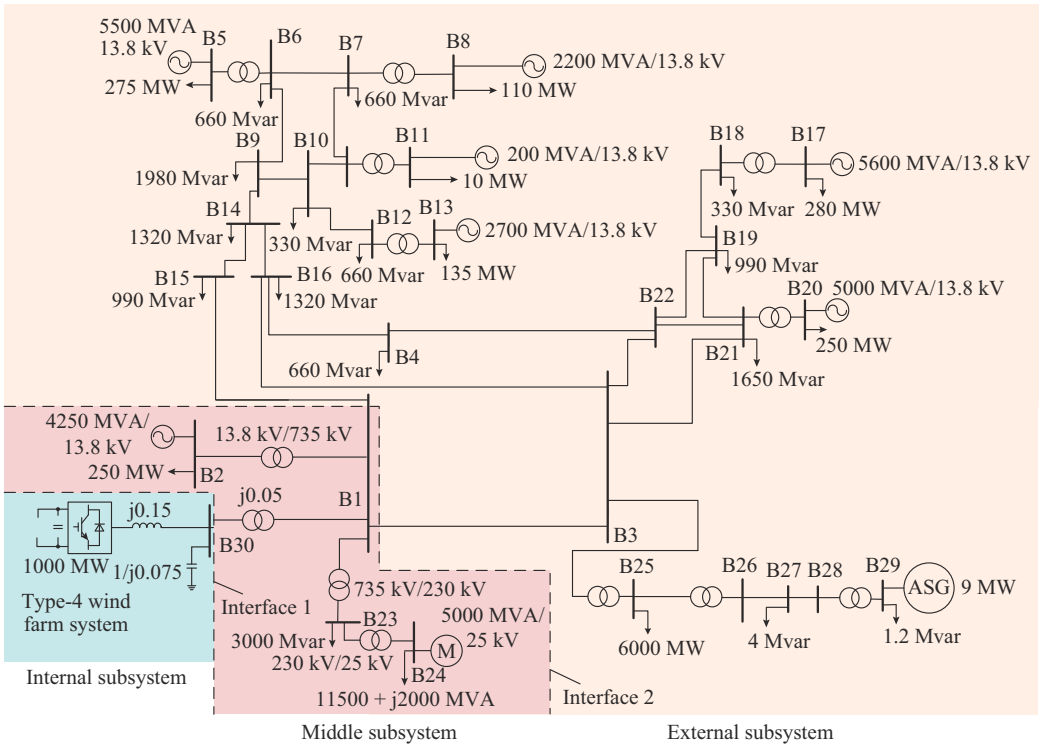

Fig. 4. Modified Hydro-Quebec system.

A. Interface 1 Identification

According to the procedure in Section II, B30 becomes the single member in interface 1. B30 itself and the integrated type-4 wind farm system form the internal subsystem.

B. Interface 2 Identification

The SSO modes of the target system are calculated as $\lambda_1 = -1.5133 \pm j2\pi \times 3.96$, $\lambda_2 = -3.6063 \pm j2\pi \times 3.35$, and $\lambda_3 = -30.3310 \pm j2\pi \times 3.234$ according to the method in [22]. λ_1 is the smallest one in view of the damping ratio, which is considered as the dominant SSO mode in this paper.

The SSO mode observability index θ_j is computed from the nodal admittance matrix $\boldsymbol{Y}(s)$ of the system. The results of the observability index are listed in Table I and obviously $S_O = \{30\}$.

TABLE I
OBSERVABILITY INDEX VALUES

Bus	θ_j	Bus	θ_j
30	0.0679	22	0.0139
23	0.0296	29	0.0132
1	0.0295	21	0.0121
24	0.0293	19	0.0111
15	0.0249	10	0.0110
25	0.0231	12	0.0090
3	0.0231	6	0.0083
26	0.0217	20	0.0078
2	0.0210	7	0.0075
16	0.0200	18	0.0061
14	0.0192	13	0.0058
27	0.0186	5	0.0054
4	0.0174	8	0.0047
9	0.0152	11	0.0047
28	0.0151	17	0.0039

Firstly, d_{kj} ($k = 30$) between interface 1 and each bus in the whole system except the internal subsystem is computed, and the results are listed in Table II. Besides, $D_k = |Z_{kk}| = 0.0702$. Then, the four buses 1, 2, 23, 24 are attributed into the middle subsystem, and other buses are all attributed to the external subsystem, i. e., $S_M = \{1, 2, 23, 24\}$, $S_E = U \backslash S_M$, where $U = \{1, 2, \ldots, 29\}$.

C. Equivalent of External Subsystem

An FDNE for the external subsystem is constructed, and the result is validated both in frequency-domain analysis and time-domain simulation.

1) Validation in Frequency Domain

In this paper, the following admittance aggregation error δ is used to measure the equivalence effect before and after the approximation.

$$\begin{cases} \boldsymbol{Y}(s) = [Y_{ij}(s)]_{N\times N} \\ \hat{\boldsymbol{Y}}(s) = [\hat{Y}_{ij}(s)]_{N\times N} \\ F_{ij} = \sqrt{\dfrac{1}{N_s}\displaystyle\sum_{i=1}^{N_s} \left| Y_{ij}(s_k) - \hat{Y}_{ij}(s_k) \right|^2} \\ \delta = \displaystyle\sum_{i=1}^{N}\sum_{j=1}^{N} F_{ij} \times 100\% \end{cases} \tag{8}$$

TABLE II
ED INDEX OF EACH BUS

Bus	d_{pj} (p.u.)	Bus	d_{pj} (p.u.)
30	0	22	0.0998
1	0.0500	19	0.0998
23	0.0551	17	0.0999
24	0.0620	10	0.1009
2	0.0688	18	0.1079
3	0.0706	7	0.1101
15	0.0759	12	0.1111
14	0.0819	13	0.1160
16	0.0851	8	0.1228
21	0.0871	4	0.1233
9	0.0877	11	0.4925
20	0.0903	26	3.3083
25	0.0923	27	9.3089
5	0.0936	28	12.7495
6	0.0951	29	13.5721

where $\hat{\boldsymbol{Y}}(s)$ is the driving point admittance matrix [12] of the external subsystem viewed from interface 2 of the original external subsystem and its FDNE, respectively; and $s_k = j2\pi f_k$, and f_k is the frequency of the k^{th} sampling point linearly distributed in [0, 120]Hz with the total number of sampling points N_s. As is presented in Fig. 5, there's a negative correlation between δ and FDNE order (details can be found in Appendix A) [23]. In this paper, FDNE order is set to be 24.

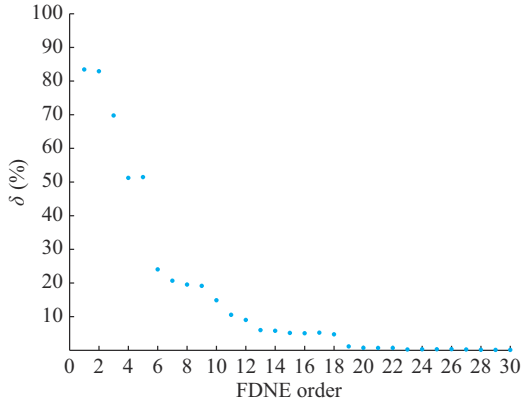

Fig. 5. Relationship between FDNE order and δ.

Figure 6(a) and (b) gives the FDNE result of $\boldsymbol{Y}(s)$ frequency response. It can be observed that in the frequency domain, the equivalent system has minor fitting error compared with the original one. Remind that the number of interface buses of the FDNE is only 1, and then $Y_{11}(s)$ and $\hat{Y}_{11}(s)$ become the only element of the matrix $\boldsymbol{Y}(s)$ and $\hat{\boldsymbol{Y}}(s)$, respectively.

2) Validation in Time-domain Simulation

The disturbance is set as follows. At $t = 0.1$ s, the output power of the wind farm at B30 is increased from 1.0 p.u. to

1.1 p.u. and at $t=0.15$ s, the power recovers to its original value. After time-domain simulation, the DC voltage of the converter is presented in Fig. 7(a) and it can be observed that the DC voltage trajectory exhibits a typical SSO phenomenon.

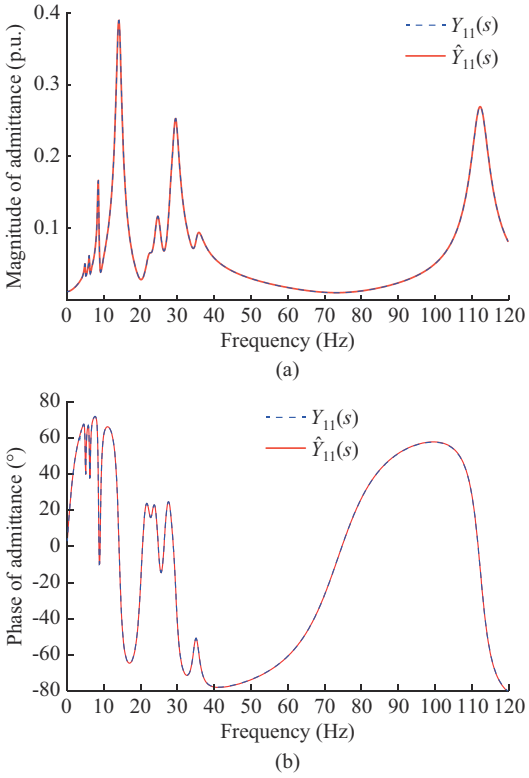

Fig. 6. FDNE results of $\boldsymbol{Y}(s)$ frequency response. (a) Magnitude-frequency characteristics. (b) Phase-frequency characteristics.

The equivalence performance can be further quantified using the 2-norm of the error signal $\varepsilon(t)=s_{eq}(t)-s_0(t)$, defined as [24]:

$$\|\varepsilon\|_2=\sqrt{\int\left|s_{eq}(t)-s_0(t)\right|^2\mathrm{d}t} \tag{9}$$

where $s_0(t)$ and $s_{eq}(t)$ are any voltage/current signal (for DC signals) or its effective value (for AC signals) before and after the equivalence, respectively. Obviously, smaller $\|\varepsilon\|_2$ value means better equivalence performance.

Here, a comparison study between the proposed method and another two-part partition method in [18] is conducted, where the remaining system is replaced by the corresponding FDNE system uniformly. The equivalence comparison results are presented in Table III, where several typical signals from the internal subsystem is given. As can be easily observed, the simulation results of the proposed method are more accurate than those of the two-part partition method [18]. The error is mainly because the dynamic characteristics in the external subsystem are not completely retained in the equivalent system. In addition, the instantaneous current waveforms injected into B2 before and after equivalence are further given in Fig. 7(b) and still their trajectories are highly consistent.

The simulation is based on a PC platform with 2.80 GHz 8 GB RAM configuration using MATLAB/Simulink. For a 1-s length simulation with time step of 2 μs, the computation time for the original system and the equivalent system with the proposed method is 191.64 s and 22.44 s, respectively, which validates that the proposed method can effectively improve the simulation efficiency.

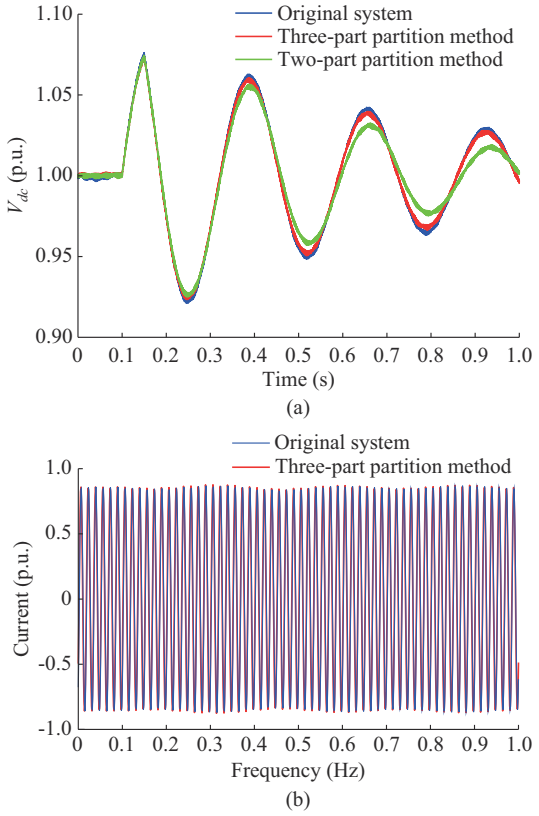

Fig. 7. Result of simulation comparison. (a) DC voltage of converter V_{dc}. (b) Instantaneous current waveforms injected into B2.

TABLE III
EQUIVALENCE COMPARISON RESULTS

Signal	Two-part partition method	Three-part partition method
Converter's DC voltage	6.4000×10^{-3}	1.8000×10^{-3}
Voltage at B30	9.4032×10^{-4}	1.1418×10^{-4}
Current via line 30-1	1.1491×10^{-3}	6.3222×10^{-4}
Wind farm power at B30	1.2544×10^{-4}	7.3337×10^{-5}

IV. CONCLUSION

This paper proposes a three-part partition method and a quantified method for interface identification in EMT simulation. The whole power grid is partitioned into the internal, the middle, and the external subsystems, where interface 1 is identified as the group of the all the grid-connected buses of these converters, whereas interface 2 is identified by the observability index and an ED-based method. For the purpose of improving the simulation accuracy, the dynamic components in middle subsystem are modeled in detail. The external subsystem is replaced by FDNE to reduce the system size and improve the simulation efficiency. Finally, the simu-

lation results verify that the equivalent system obtained from the proposed method performs better in terms of simulation accuracy than the conventional two-part partition method. The time-domain trajectory before and after the network equivalence is well consistent and the computational burden can be effectively reduced as well, such that an acceptable simulation efficiency compared with the original full system is realized.

APPENDIX A

In principle, the FDNE method approximates the frequency characteristics of the original external subsystem, driving point admittances as rational polynomials [25]. It can be realized in a variety of ways, among which the VF method is a popular one due to its robustness and stability [10]. Specific steps of VF are listed as follows.

1) Obtain frequency responses of $\boldsymbol{Y}(s)$, as introduced in (8), over a specific bandwidth.

2) Approximate $\boldsymbol{Y}(s)$ by $\hat{\boldsymbol{Y}}(s)$, whose components are n-order partial fraction expansions:

$$Y_{ij}(s) \approx \hat{Y}_{ij}(s) = \sum_{k=1}^{n} \frac{r_{k,ij}}{s - a_k} + g_{ij} + c_{ij} s \tag{A1}$$

Each polynomial consists of a set of partial fractions $r_{k,ij}/(s-a_k)$, a constant term g_{ij}, and a linear term $c_{ij}s$. Coefficients, i.e., $r_{k,ij}$, a_k, g_{ij}, and c_{ij}, are obtained by solving a set of over-determined equations [15]. Here, n is also referred to as FDNE order.

3) Carry out passivity enforcement of $\hat{\boldsymbol{Y}}(s)$ to ensure the convergence of the simulation [26].

4) Shape the equivalent network in Fig. 3 according to the fitting matrix $\hat{\boldsymbol{Y}}(s)$. The passive admittance network elements $y_{ii}(s)$ and $y_{ij}(s)$ can be determined as:

$$y_{ii}(s) = \sum_{j=1}^{N} \hat{Y}_{ij}(s) \tag{A2}$$

$$y_{ij}(s)\Big|_{i \neq j} = -\hat{Y}_{ij}(s) \tag{A3}$$

Other parameters such as C_0, R_0, R_{rk}, and R_{ck} in Fig. 3(b) can be determined by coefficients of $\hat{Y}_{ij}(s)$ in [10].

REFERENCES

[1] Y. Liang, X. Lin, A. M. Gole *et al*., "Improved coherency-based wideband equivalents for real-time digital simulators," *IEEE Transactions on Power Systems*, vol. 26, no. 3, pp. 1410-1417, Aug. 2011.

[2] H. Liu, X. Xie, J. He *et al.*, "Subsynchronous interaction between direct-drive PMSG based wind farms and weak AC networks," *IEEE Transactions on Power Systems*, vol. 32, no. 6, pp. 4708-4720, Nov. 2017.

[3] W. Chen, D. Wang, X. Xie *et al.*, "Identification of modeling boundaries for SSR studies in series compensated power networks," *IEEE Transactions on Power Systems*, vol. 32, no. 6, pp. 4851-4860, Nov. 2017.

[4] A. Semlyen and M. R. Iravani, "Frequency domain modeling of external systems in an electro-magnetic transients program," *IEEE Transactions on Power Systems*, vol. 8, no. 2, pp. 527-533, May 1993.

[5] K. Sheshyekani and B. Tabei, "Multiport frequency-dependent network equivalent using a modified matrix pencil method," *IEEE Transactions on Power Delivery*, vol. 29, no. 5, pp. 2340-2348, Oct. 2014.

[6] Y. Hu, W. Wu, B. Zhang *et al.*, "Development of an RTDS-TSA hybrid transient simulation platform with frequency dependent network equivalents," in *Proceedings of IEEE PES ISGT Europe 2013*, Lyngby, Denmark, Oct. 2013, pp. 1-5.

[7] N. G. Hingorani and M. F. Burbery, "Simulation of AC system impedance in HVDC system studies," *IEEE Transactions on Power Apparatus and Systems*, vol. PAS-89, no. 5, pp. 820-828, May 1970.

[8] K. L. Lo, L. Peng, J. F. Macqueen *et al.*, "Extended Ward equivalent of external system for on-line security analysis," in *Proceedings of 1993 2nd International Conference on Advances in Power System Control, Operation and Management (APSCOM-93)*, Hong Kong, China, Dec. 1993, pp. 54-59.

[9] A. S. Morched, J. H. Ottevangers, and L. Marti, "Multi-port frequency dependent network equivalents for the EMTP," *IEEE Transactions on Power Delivery*, vol. 8, no. 3, pp. 1402-1412, Jul. 1993.

[10] B. Gustavsen, "Computer code for rational approximation of frequency dependent admittance matrices," *IEEE Transactions on Power Delivery*, vol. 17, no. 4, pp. 1093-1098, Oct. 2002.

[11] Q. Huang and V. Vittal, "Application of electromagnetic transient-transient stability hybrid simulation to FIDVR study," *IEEE Transactions on Power Systems*, vol. 31, no. 4, pp. 2634-2646, Jul. 2016.

[12] M. Matar and R. Iravani, "A modified multiport two-layer network equivalent for the analysis of electromagnetic transients," *IEEE Transactions on Power Delivery*, vol. 25, no. 1, pp. 434-441, Jan. 2010.

[13] I. Kamwa, S. R. Samantaray, and G. Joos, "Optimal integration of disparate C37.118 PMUs in wide-area PSS with electromagnetic transients," *IEEE Transactions on Power Systems*, vol. 28, no. 4, pp. 4760-4770, Nov. 2013.

[14] X. Nie, Y. Chen, and V. Dinavahi, "Real-time transient simulation based on a robust two-layer network equivalent," *IEEE Transactions on Power Systems*, vol. 22, no. 4, pp. 1771-1781, Nov. 2007.

[15] B. Gustavsen and A. Semlyen, "Rational approximation of frequency domain responses by vector fitting," *IEEE Transactions on Power Delivery*, vol. 14, no. 3, pp. 1052-1061, Jul. 1999.

[16] Y. Zhan, X. Xie, and Y. Wang, "Impedance network model based modal observability and controllability analysis for renewable integrated power systems," *IEEE Transactions on Power Delivery*, vol. 36, no. 4, pp. 2025-2034, Aug. 2020.

[17] S. J. Schlecht and E. A. P. Habets, "Modal decomposition of feedback delay networks," *IEEE Transactions on Signal Processing*, vol. 67, no. 20, pp. 5340-5351, Oct. 2019.

[18] Y. Zhang, A. M. Gole, W. Wu *et al.*, "Development and analysis of applicability of a hybrid transient simulation platform combining TSA and EMT elements," *IEEE Transactions on Power Systems*, vol. 28, no. 1, pp. 357-366, Feb. 2013.

[19] E. Bompard, R. Napoli, and F. Xue, "Analysis of structural vulnerabilities in power transmission grids," *International Journal of Critical Infrastructure Protection*, vol. 2, no. 1-2, pp. 5-12, May 2009.

[20] E. Ghahremani and I. Kamwa, "Local and wide-area PMU-based decentralized dynamic state estimation in multi-machine power systems," *IEEE Transactions on Power Systems*, vol. 31, no. 1, pp. 547-562, Jan. 2016.

[21] C. Wang, Z. Wang, Q. Wu *et al.*, "An improved impedance/admittance analysis method considering collector subsystem transformation in converter-integrated power systems," *IEEE Transactions on Power Systems*, vol. 36, no. 6, pp. 5963-5966, Aug. 2021.

[22] H. Liu, X. Xie, and W. Liu, "An oscillatory stability criterion based on the unified *dq*-frame impedance network model for power systems with high-penetration renewables," *IEEE Transactions on Power Systems*, vol. 33, no. 3, pp. 3472-3485, May 2018.

[23] Y. Hu, W. Wu, and B. Zhang, "A fast method to identify the order of frequency-dependent network equivalents," *IEEE Transactions on Power Systems*, vol. 31, no. 1, pp. 54-62, Jan. 2016.

[24] S. Skogestad and I. Postlethwaite, *Multivariable Feedback Control: Analysis and Design.* New York: John Wiley, 2005

[25] X. Lin, A. M. Gole, and M. Yu, "A wide-band multi-port system equivalent for real-time digital power system simulators," *IEEE Transactions on Power Systems*, vol. 24, no. 1, pp. 237-249, Feb. 2009.

[26] J. Morales-Rodriguez, J. Mahseredjian, K. Sheshyekani *et al.*, "Pole-selective residue perturbation technique for passivity enforcement of FDNEs," *IEEE Transactions on Power Delivery*, vol. 33, no. 6, pp. 2746-2754, Mar. 2018.

Chenxuan Wang received the B.Eng. and the Ph.D. degrees from the College of Electrical Engineering, Zhejiang University, Hangzhou, China, in 2017 and 2022, respectively. He was a Visiting Student at Technical University of Denmark, Lyngby, Denmark, from September 2019 to September 2020. He is currently working at the Economic Research Institute of State Grid Zhejiang Electric Power Co., Ltd., Hangzhou, China. His research in-

terests include power system electromagnetic transient simulation, frequency-dependent network equivalent, and sub-synchronous oscillation analysis of grid-connected wind farms.

Weimin Zheng received the B.Eng. and the M. Eng. degrees from the College of Electrical Engineering, Zhejiang University, Hangzhou, China, in 1992 and 1995, respectively. Currently, he is working as a Senior Engineer at the Economic Research Institute of State Grid Zhejiang Electric Power Co., Ltd., Hangzhou, China. His research interests include power system planning and design.

Zhen Wang received the B.Eng., M.Eng., and Ph.D. degrees from Xi'an Jiaotong University, Xi'an, China, Zhejiang University, Hangzhou, China, and Hong Kong Polytechnic University, Hong Kong, China, in 1998, 2001, and 2009, respectively. He is currently a Full-time Professor and the Director of Institute of Power and Energy Integration & Intelligence, Zhejiang University. He was the recipient of 2014 Endeavour Research Fellowship sponsored by Australia Government and Visiting Scholar of The University of Western Australia, Perth, Australia. He is an Expert Member of IEC TC8/SC8B/JWG1 working group on Microgrid Operation and Control. He also serves as the Editor of the journal Electronics, and the Member of some topical advisory panel. His research interests include power system stability and control, renewable energy integration and voltage source converter based high-voltage direct current (VSC-HVDC) transmission.

Yangqing Dan received the B.Eng. degree from Taiyuan University of Science and Technology, Taiyuan, China, in 2005, and the M.Eng. and Ph.D. degrees from the College of Electrical and Electronic Engineering, North China Electric Power University, Beijing, China, in 2012 and 2015, respectively. Currently, he is working as a Senior Engineer at the Economic Research Institute of State Grid Zhejiang Electric Power Co., Ltd., Hangzhou, China. His research interests include power system planning and design.

Ping Ju received the B.Eng. and M.S. degrees from Southeast University, Nanjing, China, in 1982 and 1985, respectively, and the Ph.D. degree from Zhejiang University, Hangzhou, China, in 1988, all in electrical engineering. From 1994 to 1995, he was an Alexander-von-Humboldt Fellow with the University of Dortmund, Dortmund, Germany. He is currently a Professor of electrical engineering with Hohai University, Nanjing, China, and Zhejiang University. He is an IET Fellow, CSEE Fellow, IEEE SM, Chairman of IEEE PES Remote Technical Committee on Analytic Methods for Power Systems, Vice Chairman or Member of the editorial board of several international journals. His research interests include modeling and control of power systems and smart grids with renewable power generation.